Journal of Materials Chemistry A

ROYAL SOCIETY OF CHEMISTRY

PAPER

View Article Online
View Journal | View Issue

Cite this: J. Mater. Chem. A, 2023, 11, 26000

Glass-like transparent and heat-sealable films of cellulose nanoworms *via* ethanol triggered swelling of esterified cellulose†

Matias Lakovaara, [a] Juho Antti Sirviö, [a] Luyao Wang,[b] Terhi Suopajärvi,[a] Feby Pratiwi,[d] Hao Zhang, [b] Jouko Peltonen,[c] Chunlin Xu [b] and Henrikki Liimatainen *[a]

This study introduced a new and unique design of cellulose nanomaterials called cellulose nanoworms, which exhibit alluring properties for creating sustainable and advanced film structures. These nanoworms, which are being reported for the first time to the best of our knowledge, were obtained from wood-based cellulose pulp using an ethanol-induced swelling method of cellulose fibers, which were esterified with 2-octenylsuccinic anhydride in a deep eutectic solvent comprising imidazole and triethylmethylammonium chloride. When the hydrophilized fibers were exposed to ethanol, an intense ballooning phenomenon occurred, leading to the disintegration of the swollen fibers into an entangled network of cellulose nanoworms through ultrasonication. The cellulose nanoworms were further used as building blocks for the formation of films with advanced optical, surface, and thermal properties, as well as heat-sealable wrapping with desirable barrier and water resistance performance. Through the densely packed arrangement of nanoworms, the films exhibited high transparency of 92–93% without haziness or light scattering, water vapor permeability of 2.34 g μm m^{-2} d^{-1} kPa^{-1}, ultra-low root-mean-square roughness (Rq) of 2.5 nm, and good liquid water resistance, as indicated by their high mechanical strength in wet states (13.1 MPa). Thus, cellulose nanoworms served as multifunctional biomaterials with advanced and tailorable properties, making them suitable for sustainable packaging, and electronic and optic applications.

Received 21st August 2023
Accepted 13th November 2023

DOI: 10.1039/d3ta05016e

rsc.li/materials-a

Introduction

Translucent films with a green origin that meet stringent sustainability requirements are highly desired for various emerging bioeconomy applications. For this purpose, cellulose nanomaterials, such as cellulose nanocrystals (CNCs) and nanofibers (CNFs), have attracted considerable research interest because of their intrinsic ability to create uniform and continuous planar two-dimensional structures such as films, substrates, and nanopapers, with superior mechanical and barrier properties, and promising optical features.[1–6] Therefore, nanocelluloses have been intensively studied as sustainable alternatives for advanced packaging materials[5] and a greener option for electronic production. For example, nanocellulose films have been harnessed in solar cells, printable electronics, organic light-emitting diodes, and antennas.[2,7,8]

Despite many intriguing features attributed to nanocellulose films, they lack thermoformability and are difficult to shape to complex three-dimensional designs or be heat-sealed. For packaging materials, heat sealability is an important property that enables keeping microbes and other contaminants outside the package.[9,10] Typically, heat sealability is achieved using multilayered structures, in which nanocellulose barrier film is sandwiched between thermoplastic outer layers. The thermoplastic layers enable heat-induced sealing, while the nanocellulose film serves as a gas barrier.[5] However, this approach usually incorporates fossil-based plastics into the design. Alternatively, other biomaterials such as long-chain cellulose esters can be used as coatings for nanocellulose surfaces to

[a]Fibre and Particle Engineering Research Unit, University of Oulu, Oulu, Finland. E-mail: henrikki.liimatainen@oulu.fi

[b]Laboratory of Natural Materials Technology, Faculty of Science and Engineering, Åbo Akademi University, Turku, Finland

[c]Laboratory of Molecular Science and Engineering, Faculty of Science and Engineering, Åbo Akademi University, Turku, Finland

[d]Laboratory of Developmental Biology, Disease Networks Research Unit, University of Oulu, Oulu, Finland

† Electronic supplementary information (ESI) available: ESI includes additional TEM images of cellulose nanoworm suspension and original pulp after ultrasonication in ethanol, FESEM cross-sectional and surface images of nanoworm films, image of modified cellulose in water, DSC curve of modified cellulose, contact angle of films as a function of time, DRIFT spectrum of modified cellulose, schematic diagram of production process of nanoworm film, TEM images of ultrasonicated cellulose pulp, original cellulose fibers in ethanol before and after ultrasonication, XRD spectrum of modified cellulose and nanoworm film, antibacterial experiments and biodegradability test. See DOI: https://doi.org/10.1039/d3ta05016e

facilitate the heat sealability and water vapor barrier properties of multicomponent film structure.[11]

The superior mechanical and oxygen barrier properties of nanocellulose films are closely related to interfibrillar hydrogen bonding, although other interactions also contribute to film cohesion.[3,5,12–14] When water is present, the interfibrillar hydrogen bonds are affected by water molecules, causing cellulose swelling and looser film structure. Consequently, the mechanical and barrier properties of the film are significantly reduced,[1,5,15,16] and a plethora of approaches have been used to enhance the hydrophobicity and water resistance of cellulose structures. Several techniques have been reported to decrease the water sensitivity of CNF films, including direct surface modification using esterification in liquid and gas phases,[17–20] solvent exchange of water to toluene[21] and *N*,*N*-dimethylacetamide (DMAc),[22] and surface coating with paraffin wax and cellulose esters.[4,11]

Cellulose nanomaterial films possess many attractive optical properties, such as high light transmittance and transmission haze (a measure of scattered transmitted light).[23] However, random light scattering is a drawback for many electronic applications such as touchscreens and displays and must be minimized to achieve films with a super clear appearance.[24] The size of individual nanoentities is a critical parameter influencing the optical performance of nanocellulose, and harsh chemical treatments are usually used to obtain nano-objects with small lateral dimensions and narrow size distributions. For example, regioselective oxidation based on 2,2,6,6-tetramethylpiperidine-1-oxyl radical (TEMPO) – mediated or periodate oxidation has commonly been used to isolate cellulose nanofibers with diameters of just a few nanometers.[25–32]

Esterification[16,21] and silylation[19,33] have been widely studied for enhancing hydrophobicity and water resistance of cellulose structures. However, these chemical modifications often require complicated or slow processes and volatile organic solvents, such as DMAc.[34] In this study, cellulose esterification was performed using a deep eutectic solvent (DES) comprising imidazole and triethylmethylammonium chloride (TEMACl) as an alternative approach to promote cellulose hydrophobicity and thermoformability (specifically heat sealability) and release cellulose nanoentities with superior optical properties. DES can be formed from a binary or ternary combination of commonly used bulk chemicals by simple mixing and heating, allowing for the tailoring of their properties to be used as solvents, reactants, and catalysts.[35–37] Typically, DES comprises a hydrogen bond acceptor and hydrogen bond donor, which together form a fluid with a lower melting point than its components and a lower eutectic point temperature than an ideal eutectic liquid mixture.[38] Some DESs are even liquids at room temperature.[36,37] Due to the low vapor pressure and potential nontoxicity and biodegradability, DESs are attractive option for sustainable modification of biomaterials. The DES composed of imidazole and TEMACl used in this provides a nonderivatizing and nonreactive medium for cellulose esterification, as well as fast reaction kinetics and lower volatility than typical organic solvents.[39,40]

This study introduces a new and unique form of cellulose nanomaterials called cellulose nanoworms, which have attractive features for creating sustainable and advanced film structures. The nanoworms were obtained from wood-based cellulose pulp using an ethanol-induced swelling of cellulose fibers, which were esterified with 2-octenylsuccinic anhydride in DES comprising imidazole and TEMACl. When the hydrophilized fibers were exposed to ethanol, they underwent intense ballooning, leading to the disintegration of the swollen fibers into an entangled network of cellulose nanoworms through ultrasonication. The cellulose nanoworms were further harnessed as building blocks to form self-standing, hierarchical, and nanostructured films with advanced optical, surface, and thermal properties, and heat-sealable wrapping with desirable barrier and water resistance performance.

Experimental

Materials

Bleached softwood kraft pulp sheets from Metsä Fibre (Finland) were used as cellulose raw materials (77% of cellulose, 21% of hemicellulose, and 1.4% of lignin). Reference plastic films, *i.e.*, low-density polyethylene (LDPE) and polyethylene (PE), were cut from commercial plastic bags and wraps, respectively. Imidazole (purity > 98.0%), triethylmethylammoinum chloride (TEMACl) (purity > 98.0%), and 2-octenylsuccinic anhydride (OSA) (purity > 95.0%) were obtained from Tokyo Chemical Industry Co (Japan). Ethanol (purity > 96%), hydrochloric acid (HCl) (1.0 mol L^{-1}, accuracy 0.2%), and sodium hydroxide (NaOH) (0.5 mol L^{-1}, accuracy 0.2%) were obtained from VWR International (France). Calcium chloride (anhydrous powder, purity > 93%) was from Acros Organics (Belgium).

Preparation of deep eutectic solvent

DES comprising imidazole and TEMACl (molar ratio of 7 : 3) was prepared by weighing the components into a beaker glass (100 g) and heating the mixture in an oil bath at 80 °C with magnetic stirring to speed up the formation of DES. After forming a clear liquid, DES was used as a reaction medium to modify the softwood pulp.

Modification of cellulose pulp in the DES

Approximately 2 g of dry softwood pulp was ripped into small pieces and submerged into the DES. The pulp was allowed to disintegrate into the DES for approximately 10 min while continuously mixing with a magnetic stirrer. After this, the OSA reagent was added to the suspension at a molar ratio of 10 : 1 (reagent to anhydroglucose unit, AGU) and a reaction temperature of 80 °C. After 2 h, 125 mL of ethanol was added to the system to stop the reaction. The mixture was then filtered through a filter paper (pore size 4–12 μm and diameter of 90 mm) using a Büchner funnel under a vacuum pressure of −80 mbar. An additional 200 mL of ethanol was used to wash the pulp during the filtration process. Then, the pulp cake was dispersed in 250 mL of ethanol for 10 min and filtered again to remove any traces of the DES and reagent. Finally, the pulp was

washed three times with 300 mL of water–ethanol mixture in a 1 : 1 (v/v) ratio, following a similar procedure, and then dried overnight in an oven at 40 °C.

Fabrication of cellulose nanoworms and films of nanoworms

Approximately 0.3 g of modified pulp was mixed with 6 g of ethanol in a small glass vial (consistency of 5 wt%) and the suspension was sonicated for 20 min to individualize cellulose nanoworms. Hielscher UP 400s (Germany) ultrasonicator equipped with a titanium tip (diameter of 7 mm) with an amplitude of 100% and a cycle of 0.5 was used. The vial was kept in an ice-water bath during sonication to ensure proper cooling. The yield of nanoworms was analyzed by pouring a nanoworm suspension (0.3 g of dry modified pulp in ethanol with a consistency of 5 wt%) into a centrifuge tube with ethanol and centrifuging at 1300 G at 20 °C for 20 min. The yield was calculated based on eqn (3).

$$\text{Yield of nanoworms}(\%) = \frac{m_{\text{CNW}}}{m_{\text{CNW}} + m_{\text{C}}} \times 100 \quad (1)$$

where m_{CNW} is the mass of dried nanoworms in the supernatant, and m_{C} is the mass of the coarse fraction in the sediment. The results were reported in duplicate.

The cellulose nanoworm films were prepared from ethanol suspensions of cellulose nanoworms using the casting method. The sonicated suspension was poured into a Petri dish (70 mm diameter) and placed inside a desiccator with an ethanol bath at the bottom. The top valve of the desiccator was kept open, and the lid was ajar to allow the ethanol in the suspension to evaporate. The film was carefully peeled off the Petri dish after 3 days.

Analysis of the degree of substitution

The degree of substitution (DS) of esterified cellulose was determined using a modified titration method.[41,42] Before the titration, the cellulose pulp was washed with 1.0 M HCl to change carboxylic acids to acid form, and then with water to remove any traces of HCl from the dried pulp. For the titration, 0.1 g of modified pulp was immersed in a 10 mL mixture of ethanol and 0.5 M NaOH (1 : 1 v/v) and allowed to react with constant mixing for 24 h. Thereafter, 5 mL of water and 5 mL 1.0 M HCl were added to the suspension and stirred for 30 min. Finally, the suspension was back-titrated with 0.5 M NaOH using phenolphthalein as an indicator of the equivalent point of titration. The percentage number of ester groups (%substituent) was calculated using eqn (2).

$$\%\text{substituent} = \frac{[(\text{Vb}_i + \text{Vb}_t)\mu_b - (V_a \times \mu_a)]\text{M(ester group)} \times 100}{m_c} \Big/ 2 \quad (2)$$

where Vb_i is NaOH volume (L) added to the system; Vb_t is NaOH volume (L) spent in titration; μ_b is NaOH concentration (0.5 mol L^{-1}); V_a is the volume (L) of HCl added to the system; μ_a is HCl concentration (1.0 mol L^{-1}); M (ester group) is the molar weight of the substituted group (210 g mol^{-1}), and m_c is the weight (g) of the dry modified cellulose.

The %substituent values were further converted to DS values using eqn (3).

$$\text{DS} = \frac{\text{M(AGU)} \times \%\text{substituent}}{\text{M(ester group)}(100 - \%\text{substituent})} \quad (3)$$

where M(AGU) is the molar weight of anhydroglucose unit (162 g mol^{-1}). The results were calculated based on two repetitive titrations.

ATR-FTIR spectroscopy

Attenuated total reflection Fourier transform infrared (ATR-FTIR) spectroscopy was used to analyze the chemical characteristics of original and DES-modified cellulose. The spectra were recorded using Bruker Hyperion 3000 (USA), with a wavelength range of 4000–600 cm^{-1}, and 32 scans at a resolution of 4 cm^{-1}.

Optical microscopy

An optical microscope equipped with a CCD 3 MP camera (Leica DFC320, Germany) was used to reveal the morphology of the original cellulose pulp, esterified cellulose in ethanol and in dry form.

Field emission scanning electron microscopy

The structural details of cellulose nanoworms and the surface and cross-sections of the films were observed using field emission scanning electron microscopy (FESEM) (JEOL JSM-7900F, Japan) at an accelerating voltage of 5.0 kV. Platinum was used to sputter the specimens (High-Resolution Sputter Coater, Agar Scientific, UK) before analysis with a sputtering time of 30 s and a current of 40 mA.

Transmission electron microscopy

The dimensions of the cellulose nanoworms were analyzed using transmission electron microscopy (TEM, JEOL JEM-2200FS, Japan). The nanoworm suspension was first diluted with water to around 0.01 wt% and mixed at 10 000 rpm with an Ultra-Turrax mixer (IKA T25, Germany) for 1 min to achieve a homogeneous suspension. The sample was then stained with 2 wt% uranyl acetate on carbon-coated copper grids.

AFM

Atomic force microscopy (AFM) measurements were performed in ambient air at room temperature ($T = 22.3\ ^\circ\text{C} \pm 2\ ^\circ\text{C}$, relative humidity (RH) = 60% ± 5%) using a MultiMode 8 AFM (Bruker, Santa Barbara, CA) equipped with a Nanoscope V controller. Gold-coated silicon probes (NSG03 AFM probe, NT-MDT, Russia) were used in a tapping mode. The scan size used was 5 × 5 μm^2 with a resolution of 1024 × 1024 pixels. The scanning speed was 1 Hz. Nanoscope Analysis (version 1.5, Bruker) was used for data analysis.

UV-vis spectrometry

The optical transmittance of the nanoworm films was measured using a UV-vis spectrometer (Shimadzu, Japan) at a wavelength

of 200–800 nm. The film was placed between two quartz glass slides to ensure that the film was perpendicularly aligned against the incoming beam and avoided wrinkling. The absorption coefficient was calculated using the Beer–Lambert law:

$$\frac{I}{I_0} = e^{-\mu x} \quad (4)$$

where the transmittance (ratio of transmitted [I] and incoming [I_0] flux) depends on the absorption coefficient μ and the path length of the light x (m).

Contact angle measurements

Contact angle measurements were performed using Krüss DSA25 Drop Shape Analyzer (Germany). A drop of water (4 μL) was carefully placed on top of the film sample, and the drop behavior was recorded using a high-speed camera, which was analyzed using drop analyzing software. The Young–Laplace fitting method was used to extract the contact angle values 10 s after the drop was placed. For each sample, three replicates at different locations were analyzed.

Water vapor permeability analysis

The water vapor permeability (WVP) of the films was determined according to ASTM Standard E96/E96M. The measurements were done in a separate room with controlled conditions (23 °C ± 1 °C and 50% ± 2.5% RH) and the samples were conditioned in the same room 24 h before measurement. The film sample was first adjusted between two aluminum masks with a 5 cm^2 spherical hole in the center, and then the masked film was used to cover a 100 mL Schott Duran© glass bottle that had one-fourth of its volume filled with water. Finally, the bottle was capped (with a perforated cap) and a plastic seal was used to ensure a tight seal. The weight loss of the bottles was recorded at 1 h intervals for 8 h on two consecutive days to determine the weight loss–time curve. The water vapor transmission rate (WVTR) was calculated by dividing the curve slope by the exposed film area. The WVP was calculated as follows (eqn (5)):

$$\mathrm{WVP} = (\mathrm{WVTR}/S \times (R_1 - R_2)) \times h \quad (5)$$

where S is the saturation vapor pressure at the test temperature (2800 Pa at 23 °C), R_1 is the RH in the bottle expressed as a fraction (1), R_2 is the RH in the room expressed as a fraction (0.5), and h is the thickness of the film sample (m). Two measurements per film were performed.

Mechanical testing

Mechanical tests were performed on both dry (exposed to humidity at ambient conditions only) and wet films using a universal testing machine (Zwick Roell, Ulm, Germany) with a 2 kN load cell. The samples were prepared by cutting the dry film into strips with a width of 5 mm and a length of 50–70 mm. The dry films were conditioned under controlled conditions of 23 °C ± 1 °C and 50% ± 2.5% RH in the same room for 24 h before analysis. For the wet state tensile measurements, the strips were immersed in water for 24 h, with excess water removed with tissue paper before testing. The thickness of the strips was measured as an average of three random measuring points using a thickness gage (FT3, Hanatek Instruments, UK). During the tensile testing, a gage length of 40 mm was used and the strain was controlled at a speed of 5 mm min^{-1}, with a prestrain value of 0.1 and 1 MPa for dry and wet films, respectively. Young's modulus was calculated using the slope of the initial linear region of the stress–strain curve, while the ultimate tensile strength was determined as the stress at specimen fracture. The results were reported as an average of five measurements.

Differential scanning calorimetry

The glass transition temperature (T_g) of modified cellulose was determined using a differential scanning calorimeter (DSC) (Mettler Toledo DSC821e, Switzerland). The sample (2 mg) was placed in a small aluminum cup with a pierced lid and heated under nitrogen gas flow from 20 °C to 200 °C at a heating rate of 20°C min^{-1}. The sample was then cooled to 20 °C and heated again to 200 °C with a cooling/heating rate of 20 °C min^{-1}. The sample was maintained at the same temperature for 2 min before cooling and the second heating phase. T_g was determined using the second heating phase curve.

Heat-sealability testing

The heat sealability of the films was analyzed by measuring the moisture absorption of calcium chloride from the bottles covered with heat-sealed nanoworm films. First, 5.0 g of calcium chloride was placed in a 100 mL Schott Duran© glass bottle, which was then heat-sealed with the nanoworm film by pressing the film on the top of the heated bottle. As a reference, another Schott Duran© bottle (100 mL) was filled with 5.0 g of calcium chloride, but without any film sealing. Both bottles were placed into a desiccator, where water-absorbing silica gel was replaced with deionized water. The weight of the bottle was recorded once per day and cumulative moisture absorption was calculated. The heat sealability was also demonstrated by packing rise between two nanoworm film which were heat-sealed together.

Results and discussion

Cellulose esterification in DES and ethanol triggered swelling of esterified cellulose fibers

Cellulose wood pulp was first esterified using OSA, with DES of imidazole and TEMACl serving as a reaction medium and catalyst.[43–45] Typically, organic solvents, such as pyridine are used as solvents for cellulose succinylation, but the reactions are often slow and complicated.[46–50] However, DES based on imidazole and TEMACl offers a fast (reaction time of 2 h) and simple reaction medium, which is less volatile than pyridine (vapor pressures of pyridine and imidazole are 2.4 kPa at 20 °C and 0.3 Pa at 20 °C, respectively). Previous studies[39,40] have shown that DES based on imidazole and TEMACl acts as a nonderivatizing medium, meaning that neither imidazole nor TEMACl reacts with cellulose, but the imidazolium cation

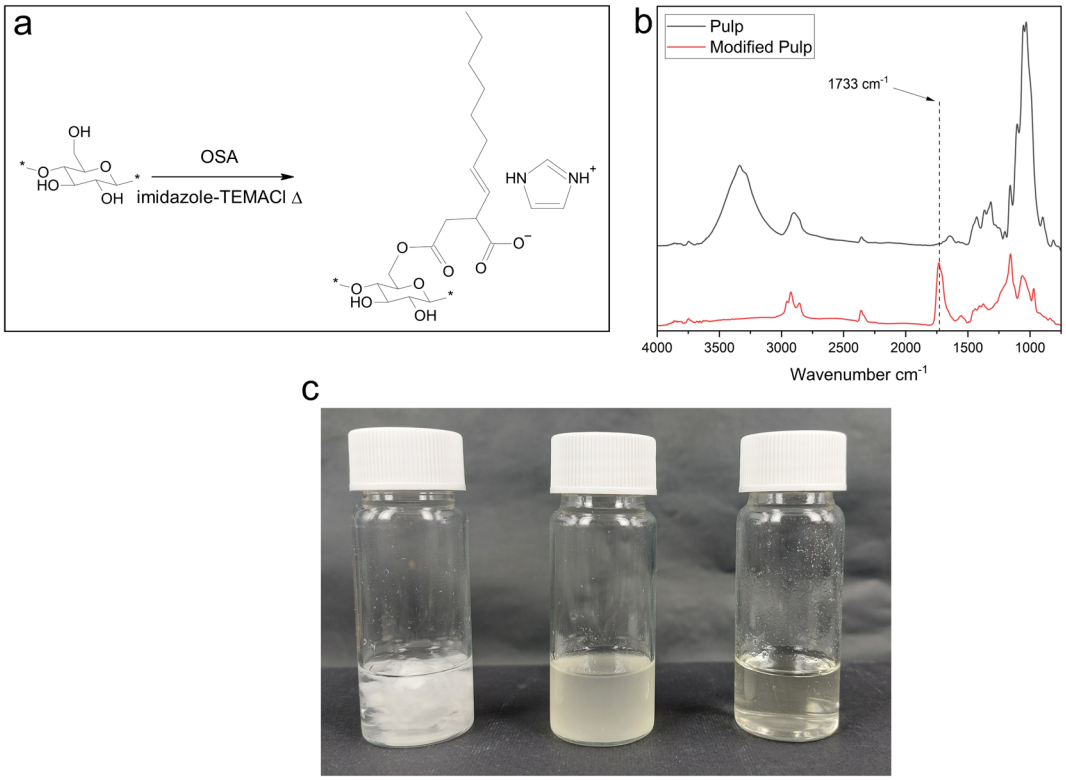

Fig. 1 (a) Esterification reaction between OSA and hydroxy groups of cellulose in DES of imidazole and TEMACl. (b) ATR-FTIR spectra of original and esterified cellulose. (c) Visual appearance of original fibers (left), DES-modified fibers (middle) and cellulose nanoworms (right).

formed as a side product is electrostatically associated with the anionic OSA chain (Fig. 1a).

Unlike the original pulp, the modified cellulose pulp showed a slightly yellowish tint after washing and drying (Fig. 1c), and it had a brittle and mechanically weak structure, which was easy to tear into smaller pieces. The esterified pulp was also highly hydrophobic; it could not be submerged in water but floated on the surface (Fig. S1†). Moreover, the reaction resulted a high DS value of 1.2.

The chemical characteristics of the pristine and modified cellulose were investigated using ATR-FTIR (Fig. 1b). The original pulp had a typical cellulose spectrum, whereas the modified pulp had a new peak at a wavenumber of 1733 cm^{-1}, which is associated with the O–C═O bond of the ester group,[46] confirming the successful esterification reaction between the OSA reagent and hydroxy groups of cellulose in DES medium. In addition, the modified pulp showed an alteration in the C–H stretching peak at wavenumber 2900 cm^{-1}, indicating the presence of the OSA's alkyl chain. Interestingly, the modified pulp did not show any O–H stretching at wavenumber 3300 cm^{-1}, and the typical C–O–C, C–O, C–H, C–O–H vibrations of cellulose between 1200 and 800 cm^{-1} were significantly altered. These findings suggested that the hydroxy groups of cellulose were esterified to a large extent, and the other characteristic vibrations at 3300 cm^{-1} and between 1200 and 800 cm^{-1} were not as strong as in the original pulp.

Furthermore, the visual appearance and behavior of pristine and esterified cellulose fibers were revealed in dry state, and ethanol suspensions (Fig. 2) using optical microscopy. The original fibers in dry form had a typical, slightly transparent fibrous structure (Fig. 2a, average diameter of ~32 μm), whereas dry modified fibers were opaque and thicker (Fig. 2b, average diameter of ~44 μm). Because of the hydrophobicity of modified cellulose fibers and the difficulty in dispersing them in water (Fig. S1†), ethanol was revealed to be an alternative suspension medium with lower polarity. Interestingly, when the modified pulp was submerged in ethanol (Fig. 2c), the fibers were easily dispersed and swelled rapidly, resulting in an intense ballooning phenomenon.[51,52] Simultaneously, the maximum diameter of modified fibers increased from 48 to 158 μm. The heterogeneously swollen fibers, which consisted of balloons separated by thin, less swollen sections, retained their fibrous structure without visible dissolution and formed a stable suspension. The original pulp fibers could not be dispersed in ethanol and formed large aggregates. As previously demonstrated with carboxymethylated fibers, the heterogenous swelling (ballooning) in water is attributed to a damaged S1 layer of the fiber wall,[51,52] indicating that OSA esterification weakened the structural integrity of the interfibrillar assembly of hydrophilized fibers when using ethanol as a suspension medium.

Isolation of cellulose nanoworms

The modified, swollen fibers were exposed to ultrasound treatment in ethanol to elucidate whether the weakened fiber

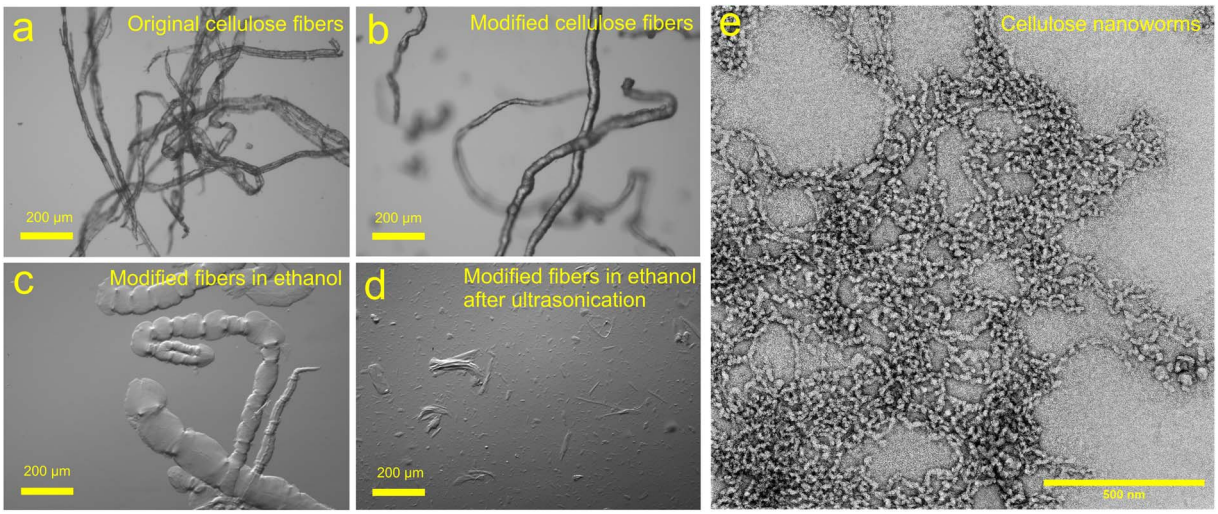

Fig. 2 Microscope images of (a) original and (b) esterified cellulose fibers in a dry form, (c) swollen esterified fibers in ethanol, and (d) residues of sonicated ethanol suspensions of esterified cellulose. (e) TEM image showing the cellulose nanoworms obtained from ethanol triggered swelling of esterified cellulose and subsequent sonication.

structure could be disintegrated into smaller, nanosized entities, similar to water-swollen fibers induced, for example, by carboxymethylation.[52] Aqueous heterogeneous (*e.g.*, carboxymethylation) and homogeneous (*e.g.*, periodate–chlorite oxidation) swelling of derivatized cellulose combined with mechanical treatments such as ultrasonication or microfluidization can liberate cellulose nanofibers or cellulose nanocrystals depending on the degree of modification and cellulose dissolution.

Fig. 2d presents the residues of ethanol suspension after the ultrasonication, which converted the turbid fiber suspension to a clear, yellowish solution, with only a minor fraction of the larger fiber fragments remaining and visible with the naked eye (Fig. 1e). Evidently, the sonication promoted the structural deformation of swollen fibers and the formation of smaller cellulose entities. Ultrasonication creates acoustic cavitation, which is the formation of microscopic vapor bubbles (cavities) in liquid media because of the local pressure drop. As the surrounding pressure increases, the cavities collapse quickly, resulting in high temperature and pressure spots in microseconds. Thus, the energy from the collapse of cavities causes fiber disintegration.[53–55]

TEM analysis was performed to reveal more closely the influence of ultrasonication on the structural alteration of esterified fibers, and to determine whether the cellulose was mainly dissolved or formed nanoscale particles (Fig. 2e). The sample comprises nanosized objects, but unlike the typical elongated and flexible structure of CNF or rod-like stiff appearance of cellulose nanocrystals (CNC), the sonicated ethanol suspension of DES-esterified cellulose consisted of an entangled network of short and relatively thick nanoscale entities, with an average lateral dimension of 18.5 nm and being linked longitudinally together. To the best of our knowledge, this kind of worm-like nanocellulose, termed here as cellulose nanoworms, has never been reported before. The cellulose nanoworms have a swollen structure similar to esterified pulp fibers in ethanol but on a smaller scale. The cellulose was covered by esterified, relatively hydrophobic OSA groups, which then interacted with ethanol resulting in a swollen surface layer and determining particle morphology on a nanoscale. In addition, the nanoworm sample contained a minor fraction of larger debris of partially disintegrated fibers (Fig. S2†). The mass yield of nanoworms was high, because 82% of the modified fibers disintegrated into nanoworms.

Films of cellulose nanoworms

The hydrophobic cellulose nanoworms were further investigated as building blocks for self-standing, hierarchical, and nanostructured films. The hydrophobicity of esterified cellulose can improve the water resistance of the films and potentially result in thermoplasticity for the cellulose. Different approaches were used in the production of films, and many attempts failed to produce a uniform film with the desired mechanical features. For example, drying the film in a room temperature, resulted in a wrinkled film surface due to excessively rapid ethanol evaporation. Finally, casting ethanol suspensions of cellulose nanoworms on a Petri dish, followed by slow drying in the presence of an ethanol atmosphere, produced homogeneous and self-standing films. Fig. 3a shows cross-sectional FESEM images of a nanoworm film consisting of similar highly swollen nano entities but more densely packed in a layered structure than observed in the dilute nanoworm suspension. More TEM and FESEM images can be found in ESI (Fig. S2–S10†).

The surface topography of the films was further analyzed using AFM imaging. The general appearance of the nanoworm films was similar to that of typical plastic films, and LDPE film was used as a reference. In addition, the surface morphology of nanoworm films was similar to that of LDPE films (Fig. 3b), but the nanoworm film exhibited drastically better surface

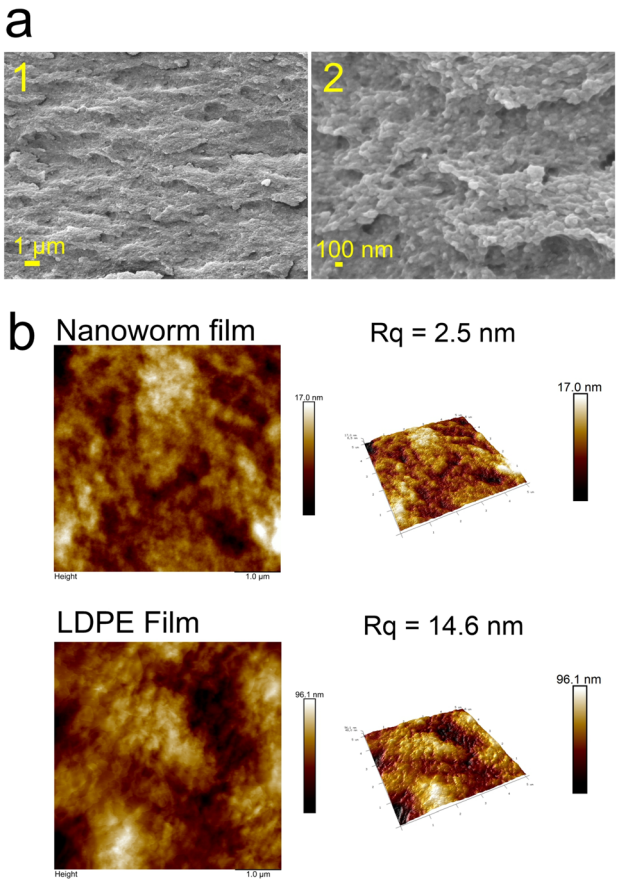

Fig. 3 (a) FESEM cross-sectional images of films of cellulose nanoworms. The images 1 and 2 are images from same the film with different magnifications (b) AFM topography images of the surface of nanoworm film (top) and LDPE films (below) from the area of 5 μm × 5 μm.

smoothness, with a root-mean-square roughness (Rq) of 2.5 nm, *i.e.*, in the scale of individual nanoworms, whereas the surface roughness for LDPE film was 14.6 nm based on the analyzed area of 5 × 5 μm. Typically, higher surface roughness values of 8–14 nm have been reported for nanocellulose films.[19,56] Hence, the nanoworm films exhibited a very dense and extremely smooth structure, which can be used in some applications, such as high-quality substrates in printed electronics.

Optical properties of the films

Fig. 4 shows that the films of cellulose nanoworms exhibit excellent optical properties with glass-like transparency and no haziness. Extremely high optical transmittance of >90% was measured over a wide wavelength range of ~400–800 nm, with a maximum transmittance of 93% at 600 nm. Previously, nanocellulose films have to exhibit optical transmittance between 42% and 90%.[25,40,57–59] Some resonance or waviness was observed in the optical spectrum at 500–800 nm, presumably because of reflection caused by the quartz glasses used in the measurement. The nanoworm films did not cause any significant light scattering, and the film background was visible when the film was laying ~15 cm above the object (Fig. 4b). These good optical properties of nanoworm films could be attributed to the small, nanoscale diameter of individualized nanoworms and the high density/low porosity of the film structure.[60] As previously stated, a small fraction of large fiber fragments were still visible among the nanoworms, but they could be removed using a separate centrifugation step to further improve the optical attributes of the films.

Wettability and water barrier properties of the films

The wettability and hydrophobicity of the films were evaluated using static contact angle measurements (Fig. 5a). The contact angle of the esterified nanoworm was 62.6°, while the LDPE film had a 95.7°, which was consistent with the value reported in the literature.[61–63] Despite the high DS of the nanoworms and their apparent poor interaction with water (Fig. S9†), the contact angle of the films was surprisingly low. However, the contact angle was almost doubled compared with that of the neat CNF film (37.8°).[39] The relatively low contact angle was related to the very low surface roughness of the films, which was significantly lower than that of LDPE (2.5 nm *vs.* 14.6 nm). For hydrophobic surfaces, the increase in surface roughness increases the contact angle because of the air pockets trapped in the surface.[64,65] For both films, the contact angle decreased slightly as the measurement proceeded (Fig. S11†) because of a tiny spreading of the water droplet on the surface. However, the nanoworm film remained intact during the measurements, indicating that no swelling of the film was observed because of a water droplet.

The water barrier performance of the films was evaluated using water vapor transmission measurements. The WVP of nanoworm films and reference CNF, LDPE, and PE films are shown in Fig. 5b.[39] The nanoworm film outperformed the neat CNF film in terms of water barrier performance (WVP of ~18.7 g μm m^{-2} d^{-1} kPa^{-1} *vs.* ~2.3 g μm m^{-2} d^{-1} kPa^{-1}), but the plastic LDPE and PE films still exhibited significantly lower vapor permeability (WVP values of 0.099 and 0.077 g μm m^{-2} d^{-1} kPa^{-1}, respectively).[5] The low WVP of nanoworm film could be attributed to the high amount of hydrophobic OSA groups attached to the cellulose structure. Water in neat CNF film breaks the tight and dense hydrogen-bonded structure, causing fiber swelling and a bulkier film structure. The OSA groups of nanoworms decrease water affinity, thereby preventing the water molecules from penetrating the film and reducing water transmission.[16,66]

Mechanical properties of the films

The mechanical properties of the nanoworm films were measured in both dry (50% RH) and wet conditions. The stress–strain curves of the films are shown in Fig. 5c, and Table 1 summarizes the tensile strength (at break), strain, and modulus values. In dry conditions, the tensile strength of the nanoworm film was 13.6 MPa, which is similar to that of the LDPE film (7–25 MPa).[63,67] However, the tensile strength was significantly lower than that of the CNF film measured in our previous study (175 MPa)[39] because of the relatively high DS of hydrophobic OSA groups on the cellulose surface. The high mechanical

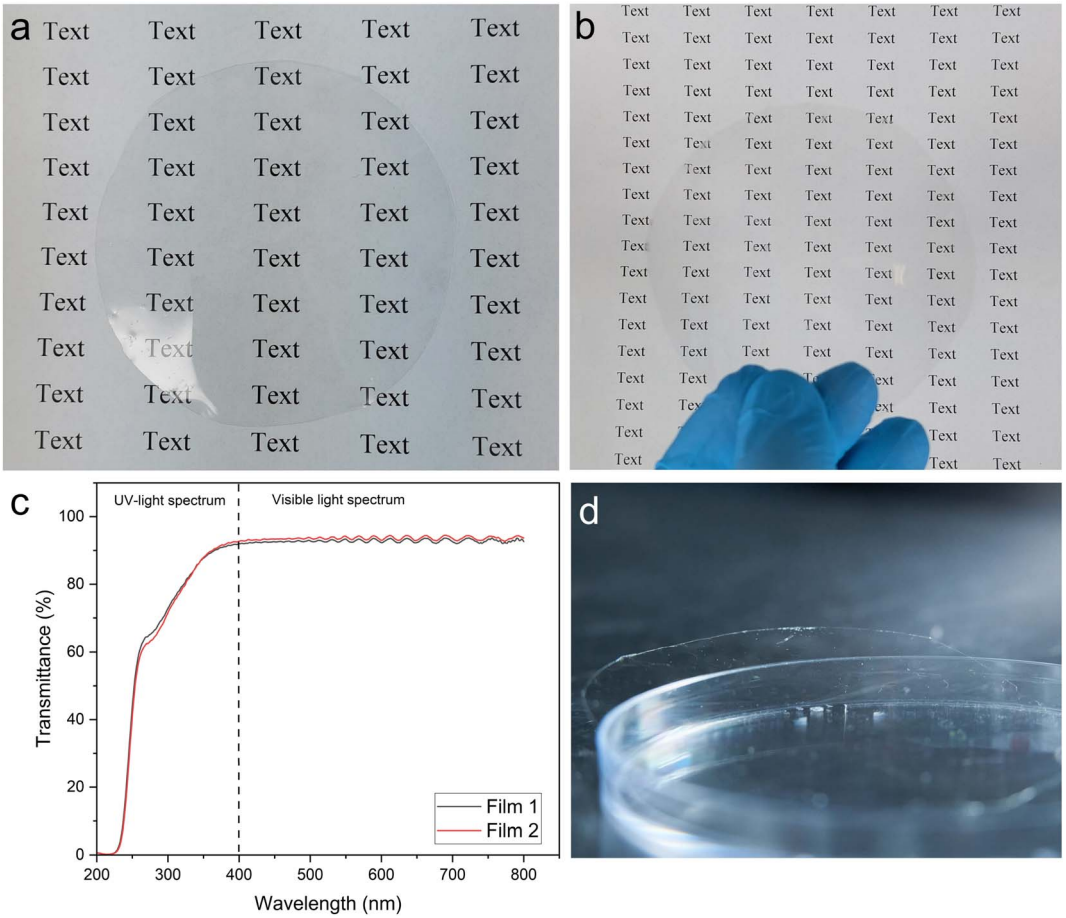

Fig. 4 (a) Visual appearance of the nanoworm film laying on top of the background and (b) ~15 cm above the background, (c) optical transmittance of two nanoworm films made from different batches of nanoworms, (d) and the film on the Petri dish.

strength of the CNF film is attributed to the abundance of interfibrillar hydrogen bonds between hydroxy groups of cellulose,[1,15] and the carbon chain of OSA reduced this interaction by replacing hydrogen bonds with weaker intermolecular bonds of OSA groups, thereby lowering the tensile strength of the film. In addition, the random orientation and short length of nanoworms may have decreased the film capacity to carry the load when subjected to stress.[16,68]

However, after exposing the dry nanoworm film to water (tensile strength in a wet state being 13.1 MPa), the tensile strength remained constant, in contrast to neat nanocellulose films, which are strongly affected by water. For example, the tensile strength decreased from 175 to 9.6 MPa with unmodified CNF film.[39] The hydrophobic interactions of the OSA side chain, which are less influenced by water than hydrogen bonds, could be attributed to the cohesion of nanoworm film in wet states.[16] The strain of films also increased at wet conditions because water acts as a plasticizer, allowing the cellulose entities to stretch more under stress.[68,69]

Thermal properties and heat sealability of the films

The thermal behavior of esterified cellulose was analyzed using DSC, which revealed a glass transition temperature (T_g) at 152 °C (Fig. S10†). Because esterification introduced a high amount of soft and bulky alkyl chains into the cellulose structure, the material's performance under heating was significantly altered compared with intact cellulose, which has no thermoplasticity or melt-processability. The OSA chains increased cellulose's free volume and inter-chain distance, allowing intermolecular chains to slide past each other.[70] As a result, a modified cellulose glass transition was observed (Fig. S12†).

The melt-processability of nanoworm films was demonstrated with heat-sealing tests by analyzing moisture absorption of calcium chloride in bottles covered with heat-sealed nanoworm films (Fig. 5d). When heat and pressure were applied during the heat-sealing process, the nanoworm film partially melted and the polymer chains diffused into each other to form a tight seal during cooling.[11] Compared with a reference without any sealing, the nanoworm film effectively decreased calcium chloride moisture uptake. After eight days, the nonsealed calcium chloride absorbed 60% of moisture relative to its original weight, while the sealed calcium chloride absorbed only 16%. Therefore, the melt-processability of nanoworm films combined with their good moisture barrier performance demonstrated their potential as adjustable, highly transparent, and bio-based packaging materials. To further demonstrate the feasibility of films as bio-derived packaging, two films were

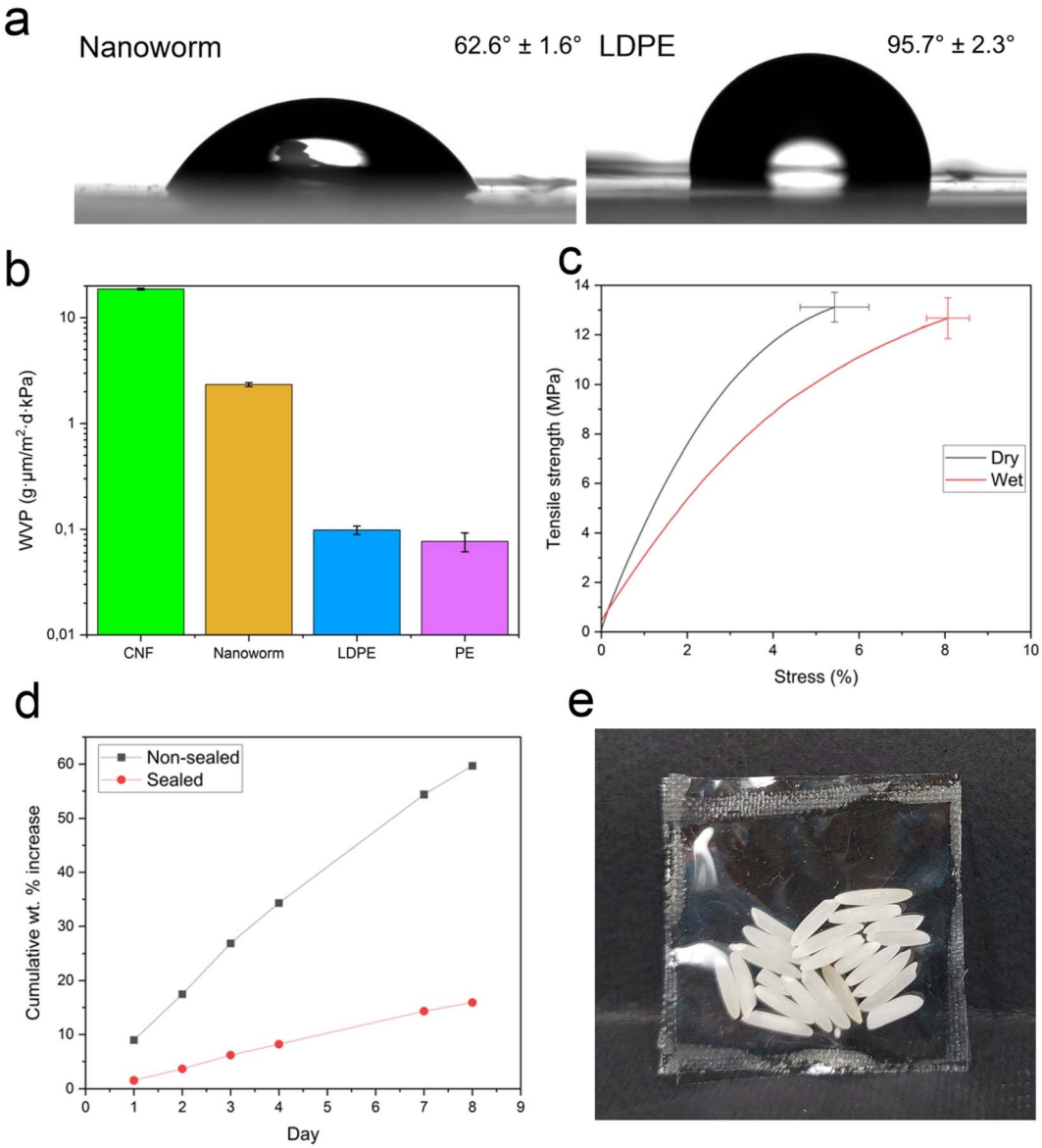

Fig. 5 (a) Water contact angles of films of cellulose nanoworms and LDPE films (at 10 s). (b) Water vapor permeability of films of nanoworms, CNF,[39] LDPE, and PE in $\log_{10}$ scale. (c) Stress–strain curves of dry and wet films of nanoworms. (d) Moisture absorption in a reference bottle and bottle covered with a heat-sealed film of nanoworms. (e) Heat-sealed package created from two nanoworm films.

Table 1 Mechanical properties of the nanoworm film at dry and wet conditions

	Tensile strength (MPa)	Strain (%)	Modulus (MPa)
Dry	13.6 ± 0.6	6.3 ± 0.8	465.1 ± 18.9
Wet	13.1 ± 0.8	8.8 ± 0.5	266.3 ± 50.4

heat-sealed together and filled with rice to form a self-standing, sealed wrapping (Fig. 5e).

Conclusions

This study introduced cellulose nanoworms, which are worm-like cellulose nanomaterials that have never been reported before, as far as we know. The esterification of cellulose with 2-octenylsuccinic anhydride, OSA, in DES, converted the cellulose pulp hydrophobic, resulting in intense ballooning when submerged in ethanol. The sonication of ethanol suspension of swollen modified cellulose fibers created an entangled network of short and relatively thick nanoworms with an average lateral dimension of 18.5 nm that were linked longitudinally together. The nanoworms were further assembled into films with an extremely smooth surface structure (root-mean-square roughness of 2.5 nm) and a contact angle of 63°. The films exhibited excellent optical properties with a transparency of 92–93% at 600 nm and WVP of 2.34 g µm m^{-2} d^{-1} kPa^{-1}. Even in the wet state, the films had a tensile strength of 13.1 MPa, which was similar to the dry state (13.6 MPa). The film also exhibited

a glass transition temperature (T_g) of 152 °C and could be heat-sealed to form a tight sealing. Therefore, the combination of melt-processability and excellent moisture barrier performance of nanostructured nanoworm films demonstrated their potential as adjustable, multifunctional biomaterials with advanced tailorable properties that could be used in sustainable packaging, electronics, and optics applications.

Author contributions

ML: conceptualization, investigation, writing – original draft. JS: conceptualization, writing – review and editing. LW: investigation – AFM imaging, writing – original draft. TS: conceptualization, investigation – biodegradability test, writing – original draft. FB: investigation – antibacterial tests, writing – original draft. HZ: investigation – XRD measurements. JP: project administration. CX: project administration. HL: writing – review and editing, project administration, funding acquisition, supervision. All authors have given approval to the final version of the manuscript.

Conflicts of interest

The authors declare no competing financial interest.

Acknowledgements

The authors acknowledge the support from the Academy of Finland project "ACNF" (325276). FESEM and TEM imaging was conducted with the support of the Centre for Material Analysis, University of Oulu, Finland. We gratefully thank the help of our laboratory staff.

References

1 C. Aulin, M. Gällstedt and T. Lindström, *Cellulose*, 2010, **17**, 559–574.
2 Z. Fang, G. Hou, C. Chen and L. Hu, *Curr. Opin. Solid State Mater. Sci.*, 2019, **23**, 100764.
3 S. S. Nair, J. Zhu, Y. Deng and A. J. Ragauskas, *Sustainable Chem. Processes*, 2014, **2**, 23.
4 M. Österberg, J. Vartiainen, J. Lucenius, U. Hippi, J. Seppälä, R. Serimaa and J. Laine, *ACS Appl. Mater. Interfaces*, 2013, **5**, 4640–4647.
5 J. Wang, D. J. Gardner, N. M. Stark, D. W. Bousfield, M. Tajvidi and Z. Cai, *ACS Sustainable Chem. Eng.*, 2018, **6**, 49–70.
6 W. Wang, R. C. Sabo, M. D. Mozuch, P. Kersten, J. Y. Zhu and Y. Jin, *J. Polym. Environ.*, 2015, **23**, 551–558.
7 Z. Fang, H. Zhu, C. Preston and L. Hu, *Transl. Mater. Res.*, 2014, **1**, 015004.
8 H. Zhu, Z. Fang, C. Preston, Y. Li and L. Hu, *Energy Environ. Sci.*, 2014, **7**, 269–287.
9 W. S. Lim, S. Y. Ock, G. D. Park, I. W. Lee, M. H. Lee and H. J. Park, *Food Packag. Shelf Life*, 2020, **26**, 100556.
10 C. Yi, T. Yuan, H. Xiao, H. Ren and H. Zhai, *Colloids Surf., A*, 2023, **666**, 131245.
11 P. Willberg-Keyriläinen, J. Vartiainen, J. Pelto and J. Ropponen, *Carbohydr. Polym.*, 2017, **170**, 160–165.
12 M. Henriksson, L. A. Berglund, P. Isaksson, T. Lindström and T. Nishino, *Biomacromolecules*, 2008, **9**, 1579–1585.
13 S. S. Ahankari, A. R. Subhedar, S. S. Bhadauria and A. Dufresne, *Carbohydr. Polym.*, 2021, **255**, 117479.
14 X. Yang, E. Jungstedt, M. S. Reid and L. A. Berglund, *Macromolecules*, 2021, **54**, 4443–4452.
15 A. J. Benítez and A. Walther, *J. Mater. Chem. A*, 2017, **5**, 16003–16024.
16 H. Sehaqui, T. Zimmermann and P. Tingaut, *Cellulose*, 2014, **21**, 367–382.
17 S. L. Balasubramaniam, A. S. Patel and B. Nayak, *Food Packag. Shelf Life*, 2020, **26**, 100587.
18 A. Khakalo, T. Mäkelä, L.-S. Johansson, H. Orelma and T. Tammelin, *ACS Appl. Bio Mater.*, 2020, **3**, 7428–7438.
19 M. S. Peresin, K. Kammiovirta, H. Heikkinen, L.-S. Johansson, J. Vartiainen, H. Setälä, M. Österberg and T. Tammelin, *Carbohydr. Polym.*, 2017, **174**, 309–317.
20 G. Rodionova, B. Hoff, M. Lenes, Ø. Eriksen and Ø. Gregersen, *Cellulose*, 2013, **20**, 1167–1174.
21 G. Rodionova, M. Lenes, Ø. Eriksen and Ø. Gregersen, *Cellulose*, 2011, **18**, 127–134.
22 W. Li, S. Wang, W. Wang, C. Qin and M. Wu, *Cellulose*, 2019, **26**, 3271–3284.
23 S. Guzman-Puyol, J. J. Benítez and J. A. Heredia-Guerrero, *Food Res. Int.*, 2022, **161**, 111792.
24 J. Tao, Z. Fang, Q. Zhang, W. Bao, M. Zhu, Y. Yao, Y. Wang, J. Dai, A. Zhang, C. Leng, D. Henderson, Z. Wang and L. Hu, *Adv. Electron. Mater.*, 2017, **3**, 1600539.
25 H. Fukuzumi, T. Saito, T. Iwata, Y. Kumamoto and A. Isogai, *Biomacromolecules*, 2009, **10**, 162–165.
26 H. Liimatainen, M. Visanko, J. A. Sirviö, O. E. O. Hormi and J. Niinimaki, *Biomacromolecules*, 2012, **13**, 1592–1597.
27 S. F. Plappert, S. Quraishi, N. Pircher, K. S. Mikkonen, S. Veigel, K. M. Klinger, A. Potthast, T. Rosenau and F. W. Liebner, *Biomacromolecules*, 2018, **19**, 2969–2978.
28 J. A. Sirviö, A. Kolehmainen, M. Visanko, H. Liimatainen, J. Niinimäki and O. E. O. Hormi, *ACS Appl. Mater. Interfaces*, 2014, **6**, 14384–14390.
29 A. Tejado, Md. N. Alam, M. Antal, H. Yang and T. G. M. van de Ven, *Cellulose*, 2012, **19**, 831–842.
30 S. Chen, Y. Song and F. Xu, *ACS Sustainable Chem. Eng.*, 2018, **6**, 5173–5181.
31 A. Isogai, T. Saito and H. Fukuzumi, *Nanoscale*, 2011, **3**, 71–85.
32 T. Saito, S. Kimura, Y. Nishiyama and A. Isogai, *Biomacromolecules*, 2007, **8**, 2485–2491.
33 L.-S. Johansson, T. Tammelin, J. M. Campbell, H. Setälä and M. Österberg, *Soft Matter*, 2011, **7**, 10917.
34 J. Sethi, M. Farooq, S. Sain, M. Sain, J. A. Sirviö, M. Illikainen and K. Oksman, *Cellulose*, 2018, **25**, 259–268.
35 B. B. Hansen, S. Spittle, B. Chen, D. Poe, Y. Zhang, J. M. Klein, A. Horton, L. Adhikari, T. Zelovich, B. W. Doherty, B. Gurkan, E. J. Maginn, A. Ragauskas, M. Dadmun, T. A. Zawodzinski, G. A. Baker,

M. E. Tuckerman, R. F. Savinell and J. R. Sangoro, *Chem. Rev.*, 2021, **121**, 1232–1285.
36 E. L. Smith, A. P. Abbott and K. S. Ryder, *Chem. Rev.*, 2014, **114**, 11060–11082.
37 Q. Zhang, K. De Oliveira Vigier, S. Royer and F. Jérôme, *Chem. Soc. Rev.*, 2012, **41**, 7108.
38 M. A. R. Martins, S. P. Pinho and J. A. P. Coutinho, *J. Solution Chem.*, 2019, **48**, 962–982.
39 M. Lakovaara, J. A. Sirviö, R. Sliz, J. Vida, T. Homola and H. Liimatainen, *Cellulose*, 2022, **29**, 9073–9087.
40 M. Lakovaara, J. A. Sirviö, M. Y. Ismail, H. Liimatainen and R. Sliz, *Cellulose*, 2021, **28**, 5433–5447.
41 G. Rodrigues Filho, D. S. Monteiro, C. D. S. Meireles, R. M. N. De Assunção, D. A. Cerqueira, H. S. Barud, S. J. L. Ribeiro and Y. Messadeq, *Carbohydr. Polym.*, 2008, **73**, 74–82.
42 R. Bhosale and R. Singhal, *Carbohydr. Polym.*, 2006, **66**, 521–527.
43 H. Nawaz, P. A. R. Pires and O. A. El Seoud, *Carbohydr. Polym.*, 2013, **92**, 997–1005.
44 P. A. R. Pires, N. I. Malek, T. C. Teixeira, T. A. Bioni, H. Nawaz and O. A. E. Seoud, *Ind. Crops Prod.*, 2015, **77**, 180–189.
45 J. A. Sirviö and M. Visanko, *J. Mater. Chem. A*, 2017, **5**, 21828–21835.
46 F. Gellerstedt and P. Gatenholm, *Cellulose*, 1999, **6**, 103–121.
47 L. V. A. Gurgel, O. K. Júnior, R. P. de F. Gil and L. F. Gil, *Bioresour. Technol.*, 2008, **99**, 3077–3083.
48 S. Hokkanen, E. Repo and M. Sillanpää, *Chem. Eng. J.*, 2013, **223**, 40–47.
49 S. Hokkanen, A. Bhatnagar and M. Sillanpää, *Water Res.*, 2016, **91**, 156–173.
50 X. Yin, C. Yu, X. Zhang, J. Yang, Q. Lin, J. Wang and Q. Zhu, *Polym. Bull.*, 2011, **67**, 401–412.
51 C. Cuissinat and P. Navard, *Macromol. Symp.*, 2006, **244**, 1–18.
52 G. Sim, M. N. Alam, L. Godbout and T. van de Ven, *Cellulose*, 2014, **21**, 4595–4606.
53 J. Levanič, K. Svedström, V. Liljeström, M. Šernek, I. G. Osojnik Črnivec, N. Poklar Ulrih and A. Haapala, *Cellulose*, 2022, **29**, 9121–9142.
54 D. V. Pinjari and A. B. Pandit, *Ultrason. Sonochem.*, 2010, **17**, 845–852.
55 J. D. Redlinger-Pohn, M. Petkovšek, K. Gordeyeva, M. Zupanc, A. Gordeeva, Q. Zhang, M. Dular and L. D. Söderberg, *Biomacromolecules*, 2022, **23**, 847–862.
56 T. Mäkelä, M. Kainlauri, P. Willberg-Keyriläinen, T. Tammelin and U. Forsström, *Microelectron. Eng.*, 2016, **163**, 1–6.
57 H. Sehaqui, A. Liu, Q. Zhou and L. A. Berglund, *Biomacromolecules*, 2010, **11**, 2195–2198.
58 Y. Qing, Z. Cai, Y. Wu, C. Yao, Q. Wu and X. Li, *Ind. Crops Prod.*, 2015, **77**, 13–20.
59 P. Li, J. A. Sirviö, A. Haapala, A. Khakalo and H. Liimatainen, *Food Hydrocolloids*, 2019, **92**, 208–217.
60 R. Pan, Y. Cheng, Y. Pei, J. Liu, W. Tian, Y. Jiang, K. Tang, J. Zhang and X. Zheng, *Cellulose*, 2023, **30**, 4813–4826.
61 S. H. Kim, H. J. Ha, Y. K. Ko, S. J. Yoon, J. M. Rhee, M. S. Kim, H. B. Lee and G. Khang, *J. Biomater. Sci., Polym. Ed.*, 2007, **18**, 609–622.
62 C.-S. Ren, K. Wang, Q.-Y. Nie, D.-Z. Wang and S.-H. Guo, *Appl. Surf. Sci.*, 2008, **255**, 3421–3425.
63 A. J. Siddiqa, K. Chaudhury and B. Adhikari, *Journal of Medicinal & Organic Chemistry*, 2015, **1**, 12.
64 D. Quéré, *Annu. Rev. Mater. Res.*, 2008, **38**, 71–99.
65 J. Wang, Y. Wu, Y. Cao, G. Li and Y. Liao, *Colloid Polym. Sci.*, 2020, **298**, 1107–1112.
66 L. C. Tomé, C. M. B. Gonçalves, M. Boaventura, L. Brandão, A. M. Mendes, A. J. D. Silvestre, C. P. Neto, A. Gandini, C. S. R. Freire and I. M. Marrucho, *Carbohydr. Polym.*, 2011, **83**, 836–842.
67 L. Bastarrachea, S. Dhawan and S. S. Sablani, *Food Eng. Rev.*, 2011, **3**, 79–93.
68 A. J. Benítez, J. Torres-Rendon, M. Poutanen and A. Walther, *Biomacromolecules*, 2013, **14**, 4497–4506.
69 J. Sethi, M. Visanko, M. Österberg and J. A. Sirviö, *Carbohydr. Polym.*, 2019, **203**, 148–156.
70 Z. Chen, J. Zhang, P. Xiao, W. Tian and J. Zhang, *ACS Sustainable Chem. Eng.*, 2018, **6**, 4931–4939.

